Orange carotenoid protein burrows into the phycobilisome to provide photoprotection.

Dvir Harris, Ofir Tal, Denis Jallet, Adjélé Wilson, Diana Kirilovsky, Noam Adir

Orange carotenoid protein burrows into the phycobilisome to provide photoprotection

Dvir Harris[a], Ofir Tal[a], Denis Jallet[b,c,1], Adjélé Wilson[b,c], Diana Kirilovsky[b,c,2], and Noam Adir[a,2]

[a]Schulich Faculty of Chemistry, Technion, Haifa 32000, Israel; [b]Institute for Integrative Biology of the Cell (I2BC), Commissariat à l'Energie Atomique (CEA), CNRS, Université Paris-Sud, Université Paris-Saclay, 91198 Gif-sur-Yvette, France; and [c]CEA, Institut de Biologie et Technologies de Saclay (iBiTec-S), 91191 Gif-sur-Yvette, France

Edited by Robert Haselkorn, University of Chicago, Chicago, IL, and approved February 3, 2016 (received for review December 4, 2015)

In cyanobacteria, photoprotection from overexcitation of photochemical centers can be obtained by excitation energy dissipation at the level of the phycobilisome (PBS), the cyanobacterial antenna, induced by the orange carotenoid protein (OCP). A single photoactivated OCP bound to the core of the PBS affords almost total energy dissipation. The precise mechanism of OCP energy dissipation is yet to be fully determined, and one question is how the carotenoid can approach any core phycocyanobilin chromophore at a distance that can promote efficient energy quenching. We have performed intersubunit cross-linking using glutaraldehyde of the OCP and PBS followed by liquid chromatography coupled to tandem mass spectrometry (LC/MS-MS) to identify cross-linked residues. The only residues of the OCP that cross-link with the PBS are situated in the linker region, between the N- and C-terminal domains and a single C-terminal residue. These links have enabled us to construct a model of the site of OCP binding that differs from previous models. We suggest that the N-terminal domain of the OCP burrows tightly into the PBS while leaving the OCP C-terminal domain on the exterior of the complex. Further analysis shows that the position of the small core linker protein ApcC is shifted within the cylinder cavity, serving to stabilize the interaction between the OCP and the PBS. This is confirmed by a ΔApcC mutant. Penetration of the N-terminal domain can bring the OCP carotenoid to within 5–10 Å of core chromophores; however, alteration of the core structure may be the actual source of energy dissipation.

photosynthesis | light harvesting | nonphotochemical quenching | cyanobacteria | cross-linking

Excess energy arriving at photochemical reaction centers (RCs) can be detrimental (1, 2), leading to loss of photosynthetic viability (photoinhibition; PI) (3, 4). Cyanobacteria have evolved several mechanisms for energy dissipation to deal with overexcitation (5, 6). The major light-harvesting complex (LHC) in cyanobacteria is the phycobilisome (PBS), a giant complex that can functionally transfer energy to two to four RCs (7–9). If overexcitation occurs rapidly, photoprotection can be achieved by decreasing the energy arriving at the RCs by increasing energy thermal dissipation (nonphotochemical quenching; NPQ) or by physical (or functional) disconnection of the PBS (10, 11). In most cyanobacterial species, NPQ is obtained by the presence a 35-kDa, water-soluble, orange carotenoid protein (OCP) (12, 13). OCP-dependent NPQ was shown to be induced (14, 15) by strong blue-green light. The OCP has two states—an inactive resting orange state (OCP^O) and an active red state (OCP^R). Upon illumination, the OCP undergoes carotenoid and protein conformational changes to yield the metastable OCP^R (16). The OCP^R binds to the PBS and significantly quenches excitation energy and PBS fluorescence (17). The OCP noncovalently binds a single keto-carotenoid chromophore, 3′-hydroxyechinenone (hECN). The high-resolution crystal structure of the OCP^O [from the cyanobacterium *Synechocystis* sp. PCC 6803; Syn; Protein Data Bank (PDB) ID code 3MG1] shows a two-domain structure connected by an unstructured loop, and revealed hECN to be concealed deep inside the protein scaffold and stabilized via hydrogen bonds from both domains (17). The N-terminal domain (residues 15–160; Nterm) is all α-helical, and the C-terminal domain (residues 196–317; Cterm) is composed of β-strands in a twisted sheet. The first 19 N-terminal amino acids (the "cap") extend over and interact with a solvent-exposed face of the β-sheet of the Cterm. The keto group of hECN is involved in hydrogen bonding with Tyr201 and Trp288 in the Cterm (13, 16, 18). It was found that the Nterm containing the carotenoid is sufficient to induce quenching activity without the presence of the Cterm (19, 20). Very recently, the structure of the N-terminal domain of the activated state of the OCP^R (denoted RCP; red carotenoid protein) was determined to high resolution, revealing that upon release of the Cterm the carotenoid molecule translates 12 Å further into the Nterm (20). By this movement, hECN is protected from the solvent, and this movement is accompanied by conformational changes that result in the change in carotenoid absorption. It can be inferred from these results that upon light activation the Cterm and Nterm of the OCP disassemble, allowing the Nterm to tightly associate with the PBS and perform its functional role of energy transfer disruption. Circular dichroism (CD) spectra of the two isolated domains suggest that each set of secondary structures is not altered by their physical separation (19), as confirmed by the RCP crystal structure for the Nterm. The length that links the Nterm to the Cterm is at most 37 residues (160–196), and thus the two domains can reach a separation of 60–80 Å, potentially leaving the Cterm unattached to the PBS (20). In the OCP^o form the Cterm prevents the OCP from binding to the PBS, and in the OCP^R the Cterm interacts with the fluorescence recovery protein (FRP), an additional component of the NPQ system. Presence of the FRP greatly enhances the reversal of OCP^R to OCP^O and unbinding of the OCP from the PBS (21).

Significance

Protection from overexcitation is one of the most important requirements of all photosynthetic organisms. Here we present a model based on coupled cross-linking/mass spectrometry and site-directed mutagenesis of the means by which the orange carotenoid protein (OCP) binds to the phycobilisome (PBS) antenna complex to avoid photodamage. The model shows that the protein must actively burrow into the complex, separating the PBS rings in the process. This penetration explains for the first time, to our knowledge, how the OCP carotenoid could approach the PBS chromophores at a distance that enables nonphotochemical quenching. However, the alteration in the core structure caused by OCP binding could also prevent energy transmission to the reaction centers.

Author contributions: D.H., D.K., and N.A. designed research; D.H., D.J., and A.W. performed research; O.T. contributed new reagents/analytic tools; D.H., O.T., D.J., A.W., D.K., and N.A. analyzed data; and D.H., D.K., and N.A. wrote the paper.

The authors declare no conflict of interest.

This article is a PNAS Direct Submission.

[1]Present address: Department of Biology, Colorado State University, Fort Collins, CO 80523.

[2]To whom correspondence may be addressed. Email: diana.kirilovsky@cea.fr or nadir@tx.technion.ac.il.

This article contains supporting information online at www.pnas.org/lookup/suppl/doi:10.1073/pnas.1523680113/-/DCSupplemental.

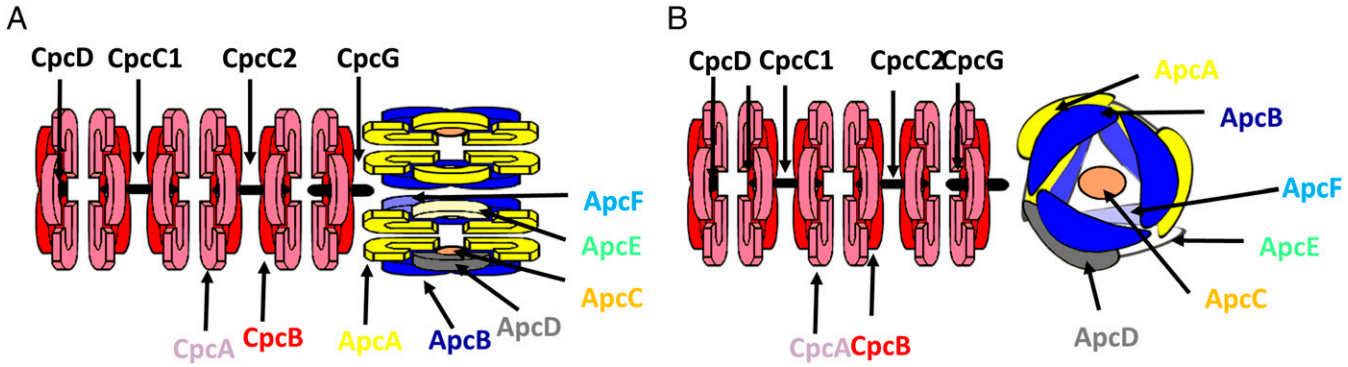

Fig. 1. Partial model of the Syn PBS. (*A*) The PBS is visualized from the direction of the thylakoid membrane. The model includes a single-basal core cylinder (including ApcA, ApcB, ApcC, ApcD, ApcE, and ApcF; colored in yellow, blue, light orange, gray, light green, and light blue, respectively) and a three-hexamer rod that includes the phycobiliproteins CpcA and CpcB (colored in pink and red, respectively) and the CpcC, CpcD, and CpcG linkers (in black). In all schematic models, linkers are shown as small objects because their position and structures are not known. Only the phycobiliprotein-type domain of ApcE is shown. (*B*) The same segment of the PBS is shown perpendicular to that in *A* (along the membrane). Colors are as in *A*.

The core of the PBS is made up of two to five cylinders (Fig. S1), each composed of four $(\alpha\beta)_3$ trimers of allophycocyanin (APC) (22, 23). Two basal core cylinders sit on top of the membrane, and contain the main form of APC (APC_{660}) and one copy each of three minor APC forms, ApcF (a β-like subunit) and ApcD and ApcE (α-like subunits; ApcE is also known as L_{CM}, and in addition to the chromophore-bearing domain also contains large linker domains of unknown position) (Fig. 1). ApcD and ApcE exhibit significant red-shifted fluorescence APC_{680} that overlaps well with the absorption of chlorophyll *a*, thus enabling efficient energy transfer from the PBS to the RC. The core is surrounded by six to eight rods containing phycocyanin (PC), which is always proximal to the core, and in some cases other phycobiliproteins (PBPs) (7). Additional non-pigmented proteins called linker or tuner proteins (LPs) are found within the empty spaces formed by APC or PC trimerization. The core contains two LPs, a small 8.5-kDa protein (ApcC) that blocks the entrance to the basal cylinders (24) and a very long extension to the ApcE subunit that is critical for core assembly (25, 26). Several models of the OCP–PBS interaction have been suggested. Blankenship and coworkers have recently used chemical cross-linking of the OCP^R to the PBS of Syn (27). Using relatively long linkers (11.4 Å), they identified four cross-links between APC and the OCP by liquid chromatography coupled to tandem mass spectrometry (LC/MS-MS) analysis. Using the OCP^O and APC crystal structures, this study suggested that the Nterm is bound between one APC_{660} and one APC_{680} trimer, bringing the hECN to 26 Å from the closest phycocyanobilin (PCB) chromophore. This model also predicted that the closest chromophore would be of the bulk APC_{660} type. However, Stadnichuk and coworkers (28, 29) have suggested that the OCP^R interacts directly with the ApcE terminal emitter in vitro, and from this it was proposed that, in vivo, proper energy propagation to the reaction center is interrupted at that site. Jallet et al. (30), using an ApcE mutant, demonstrated that the lack of the ApcE PCB also does not affect OCP-induced quenching. In addition, Jallet et al. (30) and Kuzminov et al. (31) demonstrated that single and double mutants lacking either the ApcD or ApcF subunits continue to exhibit the OCP-dependent quenching mechanism with the same kinetics. These findings have led to the conclusion that the OCP-related quenching most probably takes place at APC_{660}. van Amerongen and coworkers have shown that indeed the first site of quenching is at 660 nm and that, in cells, the total rate constant for quenching is $16 \pm 4\ ps^{-1}$ (32). Because only one of the 66 APC_{660} bilins found in the core is directly quenched by the hECN chromophore, the rate constant for molecular quenching of APC_{660} has to be at most $(240 \pm 60\ fs)^{-1}$, which is extremely fast, thus promoting very efficient quenching (80%). The exact mechanism leading to such an efficient quenching is still controversial.

In the study presented here, we have analyzed the interactions between the OCP^R and the PBS using the cross-linking mass spectrometry (MS) methodology mentioned above with the more general linker glutaraldehyde (GA). Our analysis is based on many more cross-links than previously obtained, and indicates that the OCP penetrates into the PBS core, thereby bringing hECN into close contact with multiple PCB chromophores and inducing changes in the position of the ApcC linker protein.

Results

Formation of the OCP–PBS Complex. The PBS from Syn was isolated as previously described in high-ionic-strength buffer, which is critical for the preservation of the intact and functional complex (15). Complex integrity was established by fluorescence spectroscopy (Fig. S2). The isolated PBS was incubated with isolated OCP as previously described (19). The PBS–OCP sample was passed through a second sucrose gradient to remove excess OCP, and the fluorescence measurement revealed greater than 90% quenching of the PBS fluorescence (Figs. S2 and S3).

GA Cross-Linking and Product Examination. Cross-linking with GA was performed on the highly quenched purified PBS–OCP complex according to conditions that provide a sufficient amount of the cross-linking reaction yet avoid formation of highly fixated multiple-PBS aggregates (33). The PBS–OCP complex was transferred to low-ionic-strength buffer and remained quenched due to stabilization by covalent cross-links (Fig. S3*B*). SDS/PAGE (Fig. S3*A*) revealed the appearance of new bands above the OCP, and these were used for mass spectrometry analysis (Table S1). Fluorescence analysis of cross-linked PBS–OCP transferred to low-ionic-strength buffer indicated that quenching remained at a high level, with a small amount of remaining fluorescence emitting from APC (Fig. S3*B*). The entire process was carried out independently in triplicate.

MS/MS Analysis. MS/MS analysis was executed as described in *Materials and Methods* and *SI Materials and Methods*. Exploiting the MassMatrix server (*SI Materials and Methods*, *In-Gel Proteolysis and Mass Spectrometry Analysis*) generates vast amounts of data regarding all of the possible intermolecular cross-links made between all of the different proteins found in the PBS–OCP complex. The experimental data were filtered through the statistical tools detailed in *Materials and Methods* to ensure that only statistically significant cross-links are presented. As mentioned above, this procedure was performed in triplicate to check for consistent OCP–PBS adducts. Only the top 10% among the statistically significant cross-links that were found to possess a high degree of reproducibility

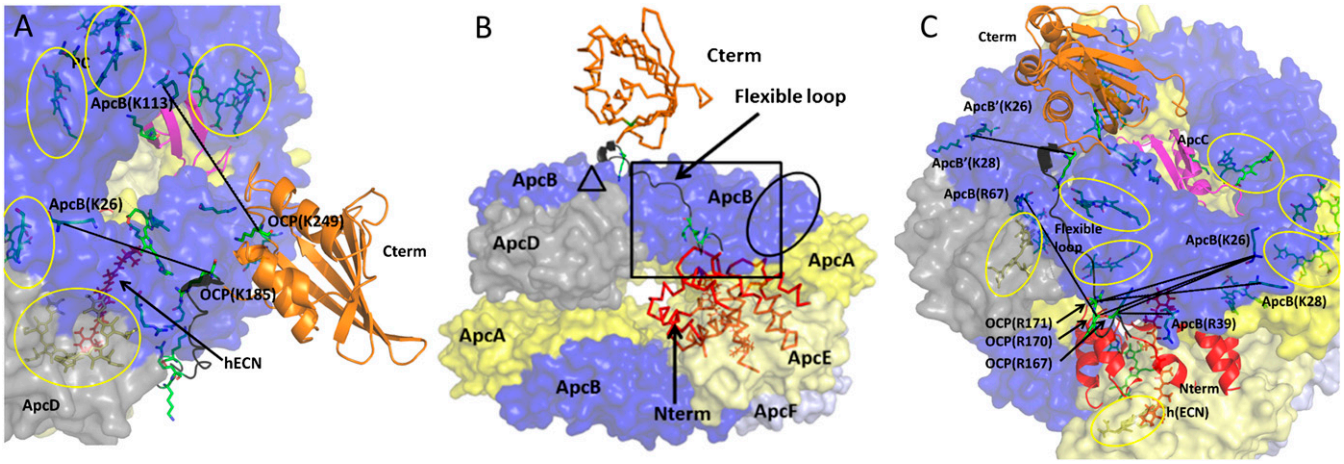

Fig. 2. Cross-link constraint-dependent model of the OCP^R–PBS complex. The OCP^R model was constructed of the Nterm (PDB ID code 4XB4; residues 20–165; red cartoon) and Cterm (based on PDB ID code 3MG1; residues 186–311; orange cartoon); the flexible domain was built using Phyre2 (residues 160–196; black). Half of a basal core cylinder was constructed from two APC trimers, associated according to Chang et al. (23). ApcA, ApcB, ApcD, ApcE, and ApcF subunits are depicted in yellow, blue, gray, wheat, and light blue surfaces, respectively. The ApcC subunit (magenta cartoon) was docked into the terminal trimer using the 1B33 structure and the alignment algorithm implemented in PyMOL. ApcB and OCP residues that participate in cross-linking are depicted in blue or red–green–blue (RGB)-colored sticks, respectively. Phycocyanobilin chromophores are depicted in Corey–Pauling–Koltun (CPK)-colored sticks and surrounded by yellow ovals. The hECN carotenoid molecule of the OCP [Nterm(hECN)] is shown as red sticks. Cross-links are shown as black lines. (*A*) The Cterm is anchored by the link between OCP(K249) and ApcB(K113). An additional link is formed by OCP(K185) at the end of the flexible loop and ApcB′(K26) on the adjacent monomer. (*B*) The flexible loop (black) crosses over the terminal trimer through the gap (highlighted by the black box) between ApcA subunits (yellow surface). The positions of the two zones of cross-linked residues on ApcB are signified by the black oval (K26/K28/R39) and triangle (R67). These residues are present in triplicate in the trimer. The Nterm is shown overlapping the trimers. This indicates that the terminal trimer must move away from the second trimer (Fig. 3). (*C*) Cross-links between flexible-loop residues R67/R70/R71/R185 and ApcB residues K26/K28/K39/K67. The OCP(R185) residue seen in *A* is shown to cross-link to ApcB′ (26), the B subunit of the adjacent monomer.

throughout the experimental repetitions (thus minimizing spurious cross-links that might appear in minor populations of the isolated PBS, or links due to nonnative interactions between two randomly interacting PBS complexes, hence reinforcing the validity of the results presented here) were taken into account while constructing models of interaction between subunits. A control experiment was performed in which the PBS underwent the same cross-linking reaction in the absence of the OCP to identify structural changes to the PBS induced by the OCP.

The most significant results of cross-linking between the OCP and PBS components and between the PBP components are shown in Table 1 and visualized in Fig. 2. Cross-links between the OCP and the PBS formed only via a relatively small segment of the protein, the flexible loop that connects the Nterm and Cterm and one residue from the Cterm that is spatially adjacent to this loop. There are a total of 5 residues in this segment, and they cross-link with 13 residues from ApcB (allophycocyanin subunit B), CpcG (rod-core linker), ApcC (core-cap linker), and CpcB (phycocyanin subunit B). This observation indicates that upon binding of the OCP^R the flexible loop is simultaneously adjacent to a core cylinder and a rod. Three of the residues found to cross-link in this present study were also identified by Zhang et al. (27); however, in this previous study, the OCP residues interacted only with ApcB (two residues) and ApcE (one residue). In the present study, the OCP interacts strongly with ApcB (five residues), ApcC (three residues), CpcG (four residues), and CpcB (one residue). The addition of more cross-linking–based constraints affords a more comprehensive model. It is quite apparent from both studies that none of the 10 potentially active residues of the Nterm (Arg, Lys, and N-terminal amine) cross-link with PBS residues. This observation would appear to be at odds with the tight binding not only of the entire OCP^R in vitro but of the functionality of the RCP (20). Eleven out of the 12 potential Cterm residues also do not form cross-links to the PBS, with residue OCP(K249) the only interacting residue.

Model of the OCP–PBS Complex Based on Cross-Linking Constraints. To try to assess how all of these cross-links can be formed simultaneously, we built a model of the OCP^R that takes into account the newly determined structure of the RCP (20). We take into account that the maximal cross-linking distance (between Cα atoms of the cross-linked residues) is ∼30 Å (33), and that the minimal distance is probably no less than 5 Å. The flexible loop (OCP residues 160–196) is depicted as an elongated peptide without secondary structure. Seven residues are lacking from all OCP structures (164–170), and so a model of the flexible loop was built using the Phyre2 server (34). This model is only a very rough approximation that is used to show the potential separation between the Cterm and Nterm upon OCP activation. The full OCP^R model was constructed by using the Nterm (PDB ID code 4XB4; residues 20–165), the Cterm (based on PDB ID code 3MG1; residues 197–311), and the flexible domain built using Phyre2 (residues 166–186). Half of a basal core cylinder was constructed from two APC trimers (based on PDB ID code 4PO5), associated according to the Chang et al. transmission

Table 1. Protein–protein cross-links identified by MS/MS analysis

OCP–ApcB	OCP–ApcC	OCP–CpcG	OCP–CpcB	ApcC–ApcF
K167–K26*	K170–K45	K170–R147	K170–K135	R2–K53
R167–R39	R171–R17	K170–R148	—	R5–K53
K170–K26	R171–K29	R171–K96	—	—
R170–R67	—	R171–R100	—	—
R171–K26	—	R171–R147	—	—
R171–K28	—	R171–R148	—	—
K185–K26	—	—	—	—
K249–K113	—	—	—	—

—, no cross-link.
*Residues correspond to the order of the subunits as denoted in the headline of each column.

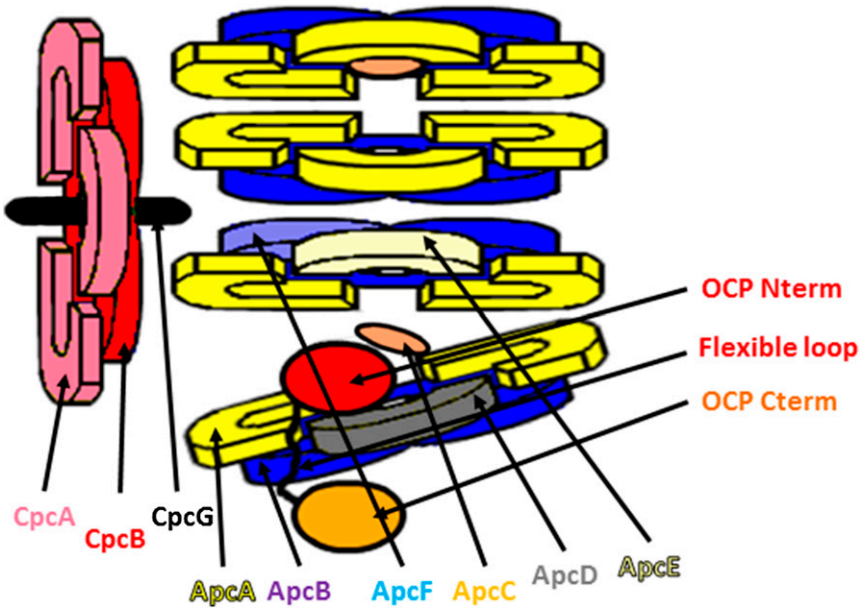

Fig. 3. Schematic model of the PBS–OCP complex. The model shows a single core cylinder composed of four trimers. The bottom two trimers have been separated by the intercalation of the OCP Nterm (dark red), connected by the flexible loop (black line) to the Cterm (dark orange) that is suspended outside the cylinder. Due to the change in the cylinder structure, ApcC (light orange) moves out of the terminal trimer and into the space near the second trimer, interacting with the Nterm and enabling cross-linking to ApcF (light blue). A single rod is shown (CpcA and CpcB in pink and red, respectively), with the CpcG linker protein (black) jutting out toward the cylinder. The end of the flexible loop closest to the Nterm must be within 30 Å of residues of CpcG (whose structure is unknown), denoted in Table 1.

electron microscopy structure (23). We assume that the OCP interacts with a basal cylinder containing AcpD and the ApcEF monomer. The ApcC subunit position was obtained by superimposing the 1B33 structure onto the terminal trimer as implemented in PyMOL (35).

OCP(K249) is the only Cterm anchor, linked to ApcB(K113). This cross-link is quite remarkable, because ApcB(K113) points outward from the APC hexamer but is on the inner circumference of the ring (Fig. 2*A*) interacting with the ApcC linker. This interaction suggests that the Cterm is positioned at the end of a core cylinder. At this position, the Cterm would be quite accessible to the FRP, which has been shown to assist in detachment of the OCP from the PBS (36). All of the other cross-links are formed with residues of the flexible loop. Obviously, on the basis of this single anchor, we cannot know exactly how the Cterm is positioned; however, the lack of significant cross-linking suggests that either it may be relatively mobile or the Lys and Arg residues may be interacting with complementary residues, thus preventing reaction with GA (under the mild conditions used here). A combination of both explanations is also possible. No cross-links occur with ApcA residues, although this subunit is rich in Lys and Arg residues, especially on the face pointing outward from the cylinder. The interactions with ApcB are located at the two ends [ApcB(K26/K28) and ApcB(K67)], with ApcB(R39) situated in the middle (Fig. 2*B*). All four residues point outward, suggesting that the loop crosses over this surface. Upon trimerization, the APC ring is actually made up of two rings: The B subunits form a contiguous ring of smaller circumference (creating the end of the core cylinder and pointing toward the cytosol), whereas the A subunits form a noncontiguous ring with larger circumference (Fig. 1*B*). Because of the lack of overlap between the A subunits, there are three gaps formed (due to the threefold symmetry of the ring) that lead to the inside of the cylinder. According to the 1B33 structure, two of these gaps are partially blocked by the ApcC capping linker protein. The role of ApcC in the OCP–PBS interaction is detailed below.

Fig. 2*C* visualizes the cross-links that are formed between the flexible loop and the PBS. As can be seen, the fact that OCP(R185) is linked to ApcB(K26) whereas OCP(R170) is linked to ApcB(R67), and taking into account the length constraints of the GA cross-linker, we arrive at the conclusion that the cross-links are formed with two B subunits, ApcB(R67) on one and ApcB(K26/K28/R39) on the other. This strengthens our conclusion that the flexible loop is near the gap separating the two monomers. These residues [OCP(K170/R171)] also interact with CpcG and CpcB, indicating that this interface is within 30 Å of the end of the basal rod cylinder that is perpendicular to the core cylinder. This conclusion is in line with recent cross-linking/MS studies on the *Thermosynechococcus vulcanus* PBS (33) and negatively stained PBS from *Anabaena* (23). In the later study, the rod would be of type Rb (rod bottom), attached to the basal cylinder. There are no structural details for the section of CpcG that is cross-linked to the flexible loop, and so these interactions are only shown schematically in the overall OCP–PBS model shown in Fig. 3. The flexible-loop residues OCP(K170/R171) also cross-link with ApcC. Using the 1B33 structure to identify the position of ApcC, the distance between the loops and ApcC(R17/K29/K45) would be beyond the 30-Å limit. However, screening for other ApcC cross-links by MS/MS revealed that when the OCP was bound to the PBS, ApcC(R2/R5) cross-links with ApcF(K53). BecauseApcF is the ApcB-like subunit that completes the ApcEF terminal monomer emitter (7, 23) and is found in the second trimer in the cylinder, this could only come about if ApcC alters its original position [this was suggested in PDB ID code 1B33 and confirmed by Tal et al. (33)], moving out of the cylinder aperture, toward the second ring (Fig. S4). This movement would have two results: It would bring ApcC(R17/K29/K45) into closer proximity with the OCP flexible loop, and would also come close to the bound Nterm. In an identical cross-linking experiment performed in the absence of the OCP, there were no observed cross-links between ApcC and ApcF.

We have explored the possibility of the Nterm pushing itself into the core cylinder through the terminal ring aperture, thereby displacing ApcC. Because of the known sizes of the Nterm (20) and aperture (7), penetration would require the entire trimer

(which is known to be quite stable) to open up significantly to afford Nterm penetration. In addition, in this scenario, it would be harder to meet all of the requirements determined by the cross-linking constraints described above.

The ΔApcC Phycobilisome Mutants. Phycobilisomes were isolated from WT, CK [containing only the APC core (37)], ΔApcC-WT, and ΔApcC-CK Syn cells. The integrity of the PBS was tested by room temperature fluorescence spectra. All of the spectra have a maximum around 667 nm with a shoulder at 680 nm (Fig. S5). However, the PBS lacking ApcC presented a slight blue shift of the maximum and slightly lower emission at 680 nm, suggesting a small destabilization [as it has been shown that properly assembled PBS components fluoresce at lower energy than isolated trimers (38, 39)] of the core of the PBS (Fig. S5). The isolated WT PBS and ΔApcC PBS were illuminated in the presence of different concentrations of the OCP under strong blue-green light in 0.5 and 0.8 M phosphate. The induced decrease of fluorescence was followed using a pulse amplitude-modulated (PAM) fluorimeter (Fig. 4 *A* and *B*). It was already shown that phosphate concentration influences the strength

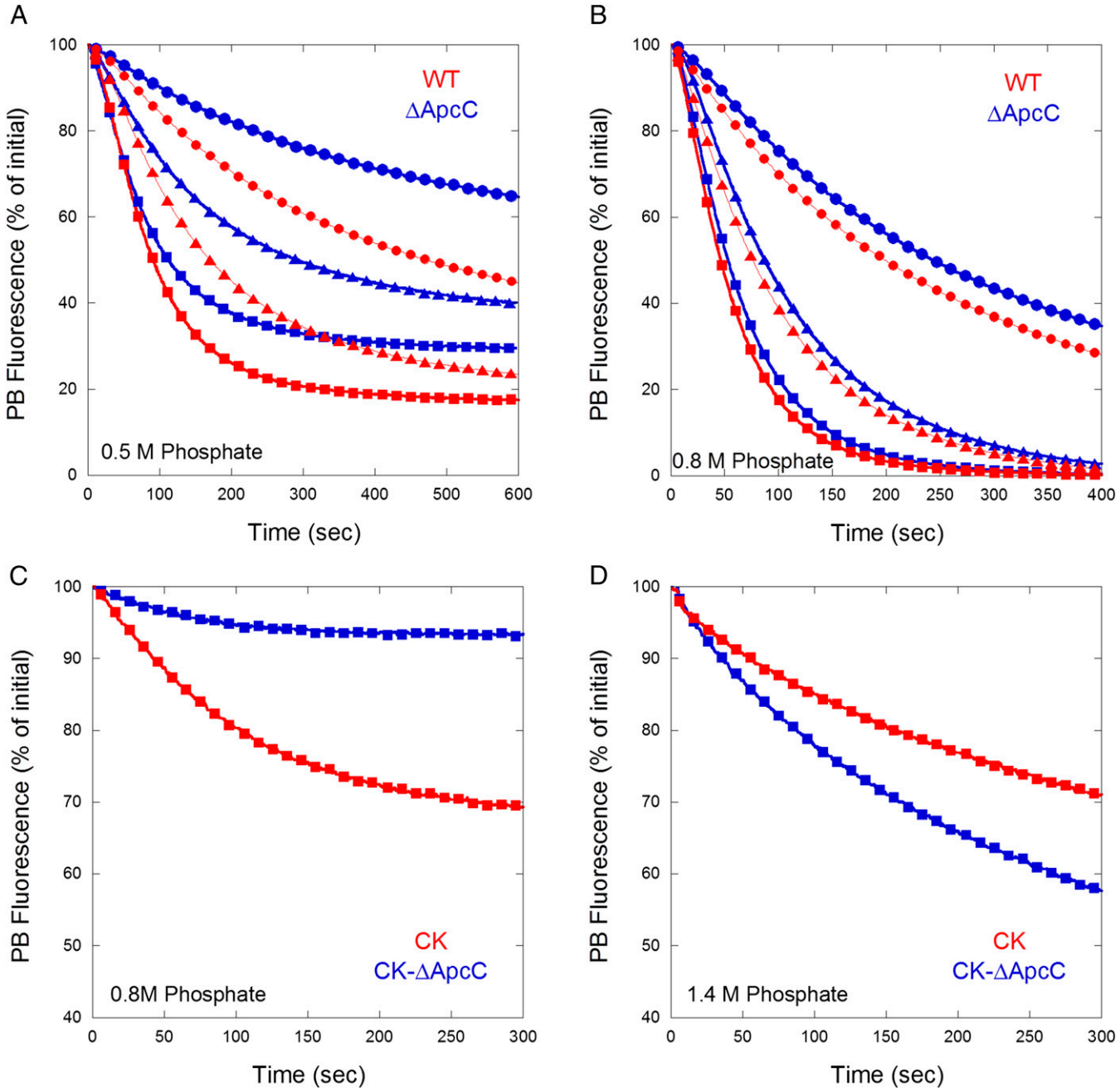

Fig. 4. ApcC depletion weakens the interaction between OCP and PBSs in vitro. Kinetics of fluorescence decrease in the WT (red) and ΔApcC (blue) PBSs (*A* and *B*) in 0.5 M (*A*) and 0.8 M phosphate buffer (*B*), and CK and CK-ΔApcC (*C* and *D*) in 0.8 M (*C*) and 1.4 M phosphate (*D*) were recorded with a PAM fluorometer. Isolated PBSs (0.012 μM) were used for each measurement. Different OCP concentrations were used, giving OCP-to-PBS ratios of 40 (squares), 20 (triangles), and 8 (circles). OCP was added in its dark, inactive orange form (OCP^O). The actinic light source, providing 900 μmol photon·m^{-2}·s^{-1} blue-green light and allowing conversion to the active red form (OCP^R), was turned on at *t* 0. Three independent experiments were performed, and the error bars (SE) are smaller than the symbols.

of OCP binding: The higher the phosphate concentration, the stronger the binding (15). Thus, the OCP induced larger quenching at 0.8 M than at 0.5 M phosphate in both types of PBS; however, with both phosphate concentrations, the decrease of fluorescence was slower and smaller in the absence of ApcC. The effect was more important at 0.5 M phosphate. The binding of the OCP to CK-PBS is largely weaker than to whole PBS, and at 0.5 M phosphate no decrease of fluorescence is detected (15). CK and ΔApcC-CK phycobilisomes were illuminated in the presence of the OCP in 0.8 and 1.4 M phosphate. As expected at 1.4 M phosphate, a stronger fluorescence quenching was observed in both types of PBS. The effect of the absence of ApcC was larger than in WT PBS. These results strongly suggest that ApcC has a role in the stabilization of OCP binding to PBS.

Discussion

Analysis of the cross-linked residues identified in this study using the available crystal structures provides a series of constraints used to suggest a model of OCP–PBS interactions not previously envisioned. Coupled with the results obtained by Zhang et al. (27), we see that Nterm Lys or Arg residues do not form cross-links to any of the PBS subunits. Even lowering the MS/MS stringency further did not reveal any Nterm cross-links to PBP or OCP residues. Because OCP^R functionality requires tight binding of the Nterm to the PBS, lack of cross-linking is not due to lack of proximity. We suggest that the lack of cross-links is due to the tight interaction between the Nterm and its binding site within the PBS, relegating the Arg and Lys residues less-reactive toward GA. This could occur if the Nterm is buried in an interface between two APC trimers in a basal cylinder in the interface with a rod. The recent structure of the PBS from *Anabaena* at ∼20-Å resolution (23) does not show the presence of a gap large enough to allow the Nterm to penetrate between APC trimers, indicating that Nterm binding significantly alters the structure of the basal cylinder, separating the terminal ring away from the second ring. Because the interactions that stabilize the APC trimer are stronger by far more than those that stabilize the hexamers of the core cylinder (interactions between two APC trimers) (7, 40), it is more likely that the Nterm burrows between rings, not through the ring aperture. Indeed, if the OCP penetrated into the cylinder via the core aperture, the absence of ApcC would actually facilitate the binding of the OCP, and faster and greater fluorescence quenching would be expected. Our results (Fig. 4) show that the opposite occurred: Slower and smaller fluorescence quenching is obtained in the absence of ApcC. Our results also show that upon OCP binding, ApcC moves and becomes closer to ApcF. It has been suggested in the past that there is structural homology between ApcC and the OCP Cterm (18). By moving into the cylinder, ApcC could stabilize Nterm binding by mimicking the Cterm. This would further explain the stability of the OCP–PBS interaction in vivo and in vitro.

The question that then arises is whether the crystal structures of the Nterm (4XB4) and APC (1B33, 4F0U, etc.) can suggest possible interaction modes when the cross-linking constraints are taken into account. Surface electrostatic potential complementarity is one characteristic that may play a role in the general formation of interaction interfaces. Indeed, based on the 1B33 structure (24), ApcC is predicted to have a surface that is almost completely positive (Fig. S6*A*), and it is indeed complementary to its binding site in the APC trimer. The calculated electrostatic potential of the Nterm is more varied, however; there is a strong positive surface along the entire length of the domain (Fig. S6*B*). As indicated above, we suggest that ApcC moves into the core cylinder upon Nterm penetration. This movement places a mostly positive object in the center of the core cylinder. One would expect that the positive surface of the Nterm would thus point away from ApcC and the center of the core. Taking into account the prediction that the linker connecting Nterm to Cterm passes over the terminal APC trimer in the gap between adjacent α-subunits, we can constrain the Nterm to a sphere of about 50 Å in diameter. The Nterm itself has a barrel-like structure 30–35 Å in width and length, and so our position has a leeway of about ±10 Å. A certain degree of rotation might also be possible.

The positive surface of ApcC forms an interaction interface with two APC monomers, each contributing two negative patches (due to residues from both the α- and β-subunits). Uncovering of these negative patches in the trimer (by the release of ApcC) could enable the positive surface of the Nterm to interact with the negative patches of the trimer. At this position there is a significant groove in the inner circumference of the trimer that can fit the Nterm nicely (Fig. S6*C*). Additional patches of negative potential on the Nterm would then match positive patches on the APC trimer. Although electrostatic complementarity is a helpful guideline for initial positioning of the interacting proteins, obtaining the precise interaction interface requires experimental data at higher resolution, which are not yet available.

Penetration of the Nterm between the terminal trimer (containing ApcD) and the second trimer (which includes the ApcEF monomer) could potentially facilitate NPQ by bringing hECN into the vicinity of the APC chromophores. This suggestion is in good accordance with the recent findings of Kuzminov et al. (31), who also proposed that the site of interaction between the OCP and the PBS is most probably located between these two trimers. It is not impossible that the position of the Nterm might actually interact with chromophores on both trimers, thus explaining the quenching of both APC_{660} and ApcE components. Our findings are not in contradiction with the results of van Amerongen and coworkers (32) indicating an APC_{660} bilin as the first site of quenching, because these trimers containing ApcD and ApcE also contain two pairs of bilins emitting at 660 nm. In light of the recent RCP (Nterm) crystal structure (20), most of the carotene is buried within the protein, with about 10 Å of protein residues insulating the conjugated polyene chain of the hECN molecule from close interactions. However, the two ends of the carotene are solvent-accessible, with the end previously bound to the Cterm being more solvent-accessible. Trimerization creates three pairs of phycocyanobilin chromophores (composed of the A84 and B84 chromophores from different monomers). These chromophore pairs may be coupled excitonically or by simple virtue of their proximity and geometry (41, 42), and the centers of these pairs face into the solvent-accessible aperture. If either or both ends of hECN could approach the bilins at a distance of 5–10 Å, one might consider direct hECN-dependent NPQ. Moreover, in the OCP^R, the ring carrying the carbonyl participates in the conjugated double-bond polyene chain extending effective π-conjugation due to the reduced ring torsions (16, 20), suggesting that either direct bilin–carotenoid energy transfer (43) or charge transfer (44) can occur. In addition, Leverenz et al. (20) suggested a possible movement of the carotenoid upon binding to the PBS partially exposing the polyene chain. This movement could enable the carotenoid to more closely approach the bilins. Nevertheless, it is also possible that a major contributor to the NPQ effect of the OCP is due to the structural modification of the core cylinder, affecting the protein environment of one or more bilin chromophores located in the area of interaction between the OCP and the PBS. This change in environment could induce interference in the native energy propagation capabilities of the affected bilin, or convert the α- or β-bilin into an energy-dissipating state, as was proposed by Wang and Moerner (42) . Further structural and spectroscopic experiments will be needed to elucidate the energy-quenching mechanism.

The mode of Nterm penetration in-between two trimers is similar to the penetration of the NblA protein, expressed in cyanobacteria under conditions of nutrient stress (45). NblA intercalates into rods (46) and core cylinders (47) into gaps between trimers, facilitating

the disassembly of the PBS. NblA consists of a helix-turn-helix motif, which also exists in the Nterm.

The Cterm, although apparently accessible, forms only a single significant cross-link to ApcB, indicating that it is mostly "floating" in solution and not bound to the PBS. Lowering the MS/MS stringency to the top 15% revealed additional Cterm cross-links to residues of ApcA, ApcD, and an external loop of ApcE (Table S2), which strengthen the suggested position. The single cross-link, however, strongly suggests that the Cterm is located on the outer surface of the basal core cylinder, and is thus available for interaction with the FRP. The finding that the OCP cross-linked with rod components (CpcG and CpcB) is also important. There certainly may be differences in the mode of attachment of the OCP^R in the presence or absence of rods (15). Thylakoid membranes are heavily covered by PBS complexes, which appear to be tightly spaced (48, 49). Because it appears that the OCP is always present in cells, it is certainly possible that it is located in its nonactive OCP^O form in close proximity to its binding site. Light-induced transformation to the OCP^R would then not require major diffusion, but one would expect some movement during its interaction with a basal cylinder. The PBSs are probably not rigid assemblies; rather, there is degree of "breathing" that occurs, with rods coupling and uncoupling from the core. The OCP could take advantage of these dynamics to squeeze its way to the core (as may occur with the NblA protein when expressed). The cross-links to the CpcG subunit are difficult to map out due to lack of structural information. It was suggested by Tal (50) and others that CpcG has two domains—the N-terminal pfam00427 domain, which was proposed to anchor the rod side, and an additional C-terminal domain, which was suggested to anchor the core side. Our cross-linking results indicate that the exact seam between the two domains (K147, K148) tends to be the most reactive toward the cross-linking manipulation with the OCP—we can therefore assume that this is the most exterior (facing outside the PBS) segment of the CpcG, although this is in the middle of the protein. It has previously been shown that when the OCP is bound to a PBS lacking rods (in vitro) fluorescence quenching still occurs, although the OCP binding is less strong (15). The presence of at least one PC hexamer is sufficient to stabilize the OCP binding (15). We have shown here that the cross-links generated between the OCP and both CpcB and CpcG in the WT PBS complex, suggest that the loop and the end of the Nterm are adjacent to the rod–core interface. These results might indicate that the role of CpcG is in positioning the Nterm correctly so that it interacts with APC_{660} and stabilizes the binding. Thus, although rods are not absolutely essential for OCP binding, they are important for its functionality in vivo.

Materials and Methods

PBS Isolation. Syn cells were grown in BG11 medium (51) at 27 °C and PBSs were isolated according to Gwizdala et al. (15) with the modifications described in *SI Materials and Methods*.

PBS–OCP Binding in Vitro. The OCP was purified and associated with isolated PBS as previously described (15). Subsequently, the PBS–OCP mixture was loaded onto a step sucrose gradient (0.25, 0.5, 0.75, 1.5 M) containing 0.9 M phosphate buffer, and ultracentrifugation was performed for 5 h at 185,000 × *g* (Beckman type 70.1 Ti rotor). The blue band located at the interface between 0.75 and 1.5 M sucrose was carefully collected and analyzed by room temperature (RT) absorbance and fluorescence spectroscopies.

Cross-Linking and Complex Isolation. Functional PBS–OCP complexes were cross-linked by 5 mM GA. The optimization of the reaction was based on previous studies (33, 52) (that demonstrated no spectroscopic effects on the absorption or fluorescence spectra of isolated PBS due to cross-linking), and the procedure is described in detail in *SI Materials and Methods*.

Analysis of Cross-Linked Adducts by Mass Spectrometry. All MS/MS procedures were done at the Smoler Proteomics Center at the Technion, and the bioinformatic analysis was done as previously described (33). Detailed results of the MS/MS analysis are detailed in depth in *SI Materials and Methods*.

Fluorescence and Absorbance Measurements. Fluorescence measurements were carried out with a HORIBA Jobin Yvon spectrofluorometer at RT with excitation and emission slits of ±2.5 nm. Absorbance measurements were carried out with a Shimadzu spectrophotometer at RT.

Modeling and Computational Tools. Predictions of protein structures, when needed, were carried out using Phyre2 (34). Identification of cross-linked peptides was done with MassMatrix (53, 54), whereas general identification was done with SEQUEST (Thermo Finnigan). All structure manipulations were done using PyMOL (35) and Chimera (55).

Construction of ΔApcC Mutants. The *apc* operon containing the genes *apcA*, *apcB*, and *apcC* was amplified using the synthetic oligonucleotides FABC-NotI (5′-CAAAGCGGCCGCGTAAATTCTGCTGGCGATCG-3′) and RABC-XhoI (5′-GGAGAACTCGAGGGTCATCAATGAGGCAGTC-3′) and genomic Syn DNA as template. The amplified fragment was cloned between the NotI and XhoI sites of the Bluescript SK plasmid. The obtained SK-apcABC plasmid was digested by NdeI and MfeI to delete a portion of the *apcC* gene, which was replaced by an Sp/Smr cassette. The blunt-ended Sp/Sm cassette (digested by HincII) was cloned between the NdeI and MfeI sites. The mutation was confirmed by enzymatic digestion and sequencing. The plasmid was used to transform WT and CK Syn cells. The construction of the CK mutant was described previously (37).

Fluorescence Measurements. Fluorescence quenching and recovery were monitored with a pulse amplitude-modulated fluorimeter (101/102/103-PAM; Walz). All measurements were carried out in a stirred cuvette of 1-cm diameter. Typically, the fluorescence quenching was induced by 900 μmol photon·m^{-2}·s^{-1} of blue-green light (400–550 nm) at 23 °C.

ACKNOWLEDGMENTS. We thank the staff of the Smoler Proteomics Center for assistance in developing the methods for coupled cross-linking/MS of the PBS proteins. We thank Dr. Ghada Ajlani for the gift of the CK *Synechocystis* mutant. We thank Sandrine Cot for technical assistance. This study was supported by the Israel Science Foundation (1576/12) and the US-Israel Bi-National Science Fund (2009406). We also acknowledge support from the Nancy and Stephen Grand Technion Energy Program (GTEP) and the Technion Russell Berrie Nanotechnology Institute (RBNI). The research in D.K.'s laboratory was supported by grants from the Agence Nationale de la Recherche (ANR; Project CYANOPROTECT), the Centre National de la Recherche Scientifique (CNRS), and the Commissariat à l'Energie Atomique (CEA).

1. Allahverdiyeva Y, Suorsa M, Tikkanen M, Aro EM (2015) Photoprotection of photosystems in fluctuating light intensities. *J Exp Bot* 66(9):2427–2436.
2. Niyogi KK, Truong TB (2013) Evolution of flexible non-photochemical quenching mechanisms that regulate light harvesting in oxygenic photosynthesis. *Curr Opin Plant Biol* 16(3):307–314.
3. Adir N, Zer H, Shochat S, Ohad I (2003) Photoinhibition—A historical perspective. *Photosynth Res* 76(1–3):343–370.
4. Xu DQ, Chen Y, Chen GY (2015) Light-harvesting regulation from leaf to molecule with the emphasis on rapid changes in antenna size. *Photosynth Res* 124(2): 137–158.
5. Bailey S, Grossman A (2008) Photoprotection in cyanobacteria: Regulation of light harvesting. *Photochem Photobiol* 84(6):1410–1420.
6. Muramatsu M, Hihara Y (2012) Acclimation to high-light conditions in cyanobacteria: From gene expression to physiological responses. *J Plant Res* 125(1): 11–39.
7. Adir N (2005) Elucidation of the molecular structures of components of the phycobilisome: Reconstructing a giant. *Photosynth Res* 85(1):15–32.
8. Marx A, David L, Adir N (2014) Piecing together the phycobilisome. *The Structural Basis of Biological Energy Generation (Advances in Photosynthesis and Respiration)*, ed Hohmann-Marriott MF (Springer, Dordrecht, The Netherlands), pp 59–76.
9. Watanabe M, Ikeuchi M (2013) Phycobilisome: Architecture of a light-harvesting supercomplex. *Photosynth Res* 116(2–3):265–276.
10. Derks A, Schaven K, Bruce D (2015) Diverse mechanisms for photoprotection in photosynthesis. Dynamic regulation of photosystem II excitation in response to rapid environmental change. *Biochim Biophys Acta* 1847(4–5):468–485.
11. Kirilovsky D, Kaňa R, Prášil O (2014) Mechanisms modulating energy arriving at reaction centers in cyanobacteria. *Non-Photochemical Quenching and Energy Dissipation in Plants, Algae and Cyanobacteria (Advances in Photosynthesis and Respiration)*, eds Demmig-Adams B, Garab G, Govindjee (Springer, Dordrecht, The Netherlands), Vol 40, pp 471–501.
12. Kirilovsky D (2015) Modulating energy arriving at photochemical reaction centers: Orange carotenoid protein-related photoprotection and state transitions. *Photosynth Res* 126(1):3–17.

13. Kirilovsky D, Kerfeld CA (2013) The orange carotenoid protein: A blue-green light photoactive protein. *Photochem Photobiol Sci* 12(7):1135–1143.
14. Wilson A, et al. (2006) A soluble carotenoid protein involved in phycobilisome-related energy dissipation in cyanobacteria. *Plant Cell* 18(4):992–1007.
15. Gwizdala M, Wilson A, Kirilovsky D (2011) In vitro reconstitution of the cyanobacterial photoprotective mechanism mediated by the orange carotenoid protein in *Synechocystis* PCC 6803. *Plant Cell* 23(7):2631–2643.
16. Wilson A, et al. (2008) A photoactive carotenoid protein acting as light intensity sensor. *Proc Natl Acad Sci USA* 105(33):12075–12080.
17. Wilson A, et al. (2010) Structural determinants underlying photoprotection in the photoactive orange carotenoid protein of cyanobacteria. *J Biol Chem* 285(24): 18364–18375.
18. Wilson A, Punginelli C, Couturier M, Perreau F, Kirilovsky D (2011) Essential role of two tyrosines and two tryptophans on the photoprotection activity of the orange carotenoid protein. *Biochim Biophys Acta* 1807(3):293–301.
19. Leverenz RL, et al. (2014) Structural and functional modularity of the orange carotenoid protein: Distinct roles for the N- and C-terminal domains in cyanobacterial photoprotection. *Plant Cell* 26(1):426–437.
20. Leverenz RL, et al. (2015) A 12 Å carotenoid translocation in a photoswitch associated with cyanobacterial photoprotection. *Science* 348(6242):1463–1466.
21. Gwizdala M, Wilson A, Omairi-Nasser A, Kirilovsky D (2013) Characterization of the *Synechocystis* PCC 6803 fluorescence recovery protein involved in photoprotection. *Biochim Biophys Acta* 1827(3):348–354.
22. Adir N (2008) Structure of the phycobilisome antennae in cyanobacteria and red algae. *Photosynthetic Protein Complexes: A Structural Approach*, ed Fromme P (Wiley, Weinheim, Germany), pp 243–274.
23. Chang L, et al. (2015) Structural organization of an intact phycobilisome and its association with photosystem II. *Cell Res* 25(6):726–737.
24. Reuter W, Wiegand G, Huber R, Than ME (1999) Structural analysis at 2.2 Å of orthorhombic crystals presents the asymmetry of the allophycocyanin-linker complex, AP.LC7.8, from phycobilisomes of *Mastigocladus laminosus*. *Proc Natl Acad Sci USA* 96(4):1363–1368.
25. Capuano V, Braux AS, Tandeau de Marsac N, Houmard J (1991) The "anchor polypeptide" of cyanobacterial phycobilisomes. Molecular characterization of the *Synechococcus* sp. PCC 6301 apce gene. *J Biol Chem* 266(11):7239–7247.
26. Liu LN, Chen XL, Zhang YZ, Zhou BC (2005) Characterization, structure and function of linker polypeptides in phycobilisomes of cyanobacteria and red algae: An overview. *Biochim Biophys Acta* 1708(2):133–142.
27. Zhang H, et al. (2014) Molecular mechanism of photoactivation and structural location of the cyanobacterial orange carotenoid protein. *Biochemistry* 53(1):13–19.
28. Stadnichuk IN, et al. (2012) Site of non-photochemical quenching of the phycobilisome by orange carotenoid protein in the cyanobacterium *Synechocystis* sp. PCC 6803. *Biochim Biophys Acta* 1817(8):1436–1445.
29. Stadnichuk IN, et al. (2015) Electronic coupling of the phycobilisome with the orange carotenoid protein and fluorescence quenching. *Photosynth Res* 124(3):315–335.
30. Jallet D, Gwizdala M, Kirilovsky D (2012) ApcD, ApcF and ApcE are not required for the orange carotenoid protein related phycobilisome fluorescence quenching in the cyanobacterium *Synechocystis* PCC 6803. *Biochim Biophys Acta* 1817(8): 1418–1427.
31. Kuzminov FI, Bolychevtseva YV, Elanskaya IV, Karapetyan NV (2014) Effect of APCD and APCF subunits depletion on phycobilisome fluorescence of the cyanobacterium *Synechocystis* PCC 6803. *J Photochem Photobiol B* 133:153–160.
32. Tian L, et al. (2012) Picosecond kinetics of light harvesting and photoprotective quenching in wild-type and mutant phycobilisomes isolated from the cyanobacterium *Synechocystis* PCC 6803. *Biophys J* 102(7):1692–1700.
33. Tal O, Trabelcy B, Gerchman Y, Adir N (2014) Investigation of phycobilisome subunit interaction interfaces by coupled cross-linking and mass spectrometry. *J Biol Chem* 289(48):33084–33097.
34. Kelley LA, Mezulis S, Yates CM, Wass MN, Sternberg MJ (2015) The Phyre2 web portal for protein modeling, prediction and analysis. *Nat Protoc* 10(6):845–858.
35. DeLano WL (2002) The PyMOL Molecular Graphics System. Available at www.pymol.org.
36. Sutter M, et al. (2013) Crystal structure of the FRP and identification of the active site for modulation of OCP-mediated photoprotection in cyanobacteria. *Proc Natl Acad Sci USA* 110(24):10022–10027.
37. Ajlani G, Vernotte C, DiMagno L, Haselkorn R (1995) Phycobilisome core mutants of *Synechocystis* PCC 6803. *Biochim Biophys Acta* 1231(2):189–196.
38. MacColl R (2004) Allophycocyanin and energy transfer. *Biochim Biophys Acta* 1657(2-3):73–81.
39. David L, Marx A, Adir N (2011) High-resolution crystal structures of trimeric and rod phycocyanin. *J Mol Biol* 405(1):201–213.
40. Adir N, Dobrovetsky Y, Lerner N (2001) Structure of c-phycocyanin from the thermophilic cyanobacterium *Synechococcus vulcanus* at 2.5 Å: Structural implications for thermal stability in phycobilisome assembly. *J Mol Biol* 313(1):71–81.
41. McGregor A, Klartag M, David L, Adir N (2008) Allophycocyanin trimer stability and functionality are primarily due to polar enhanced hydrophobicity of the phycocyanobilin binding pocket. *J Mol Biol* 384(2):406–421.
42. Wang Q, Moerner WE (2015) Dissecting pigment architecture of individual photosynthetic antenna complexes in solution. *Proc Natl Acad Sci USA* 112(45): 13880–13885.
43. Berera R, et al. (2012) The photophysics of the orange carotenoid protein, a light-powered molecular switch. *J Phys Chem B* 116(8):2568–2574.
44. Tian L, et al. (2011) Site, rate, and mechanism of photoprotective quenching in cyanobacteria. *J Am Chem Soc* 133(45):18304–18311.
45. Grossman AR, et al. (1993) The phycobilisome, a light-harvesting complex responsive to environmental conditions. *Microbiol Rev* 57(3):725–749.
46. Dines M, et al. (2008) Structural, functional, and mutational analysis of the NblA protein provides insight into possible modes of interaction with the phycobilisome. *J Biol Chem* 283(44):30330–30340.
47. Sendersky E, et al. (2015) The proteolysis adaptor, NblA, is essential for degradation of the core pigment of the cyanobacterial light-harvesting complex. *Plant J* 83(5): 845–852.
48. Liu LN, et al. (2008) Watching the native supramolecular architecture of photosynthetic membrane in red algae: Topography of phycobilisomes and their crowding, diverse distribution patterns. *J Biol Chem* 283(50):34946–34953.
49. Anderson LK, Toole CM (1998) A model for early events in the assembly pathway of cyanobacterial phycobilisomes. *Mol Microbiol* 30(3):467–474.
50. Tal O (2014) Investigations of the interactions leading to phycobilisome assembly. PhD thesis (Technion, Haifa, Israel).
51. Herdman M (1973) Mutations arising during transformation in the blue-green alga *Anacystis nidulans*. *Mol Gen Genet* 120(4):369–378.
52. David L, et al. (2014) Structural studies show energy transfer within stabilized phycobilisomes independent of the mode of rod-core assembly. *Biochim Biophys Acta* 1837(3):385–395.
53. Xu H, Freitas MA (2009) Automated diagnosis of LC-MS/MS performance. *Bioinformatics* 25(10):1341–1343.
54. Xu H, Hsu PH, Zhang L, Tsai MD, Freitas MA (2010) Database search algorithm for identification of intact cross-links in proteins and peptides using tandem mass spectrometry. *J Proteome Res* 9(7):3384–3393.
55. Pettersen EF, et al. (2004) UCSF Chimera—A visualization system for exploratory research and analysis. *J Comput Chem* 25(13):1605–1612.